



Elucidating Active CO–Au Species on Au/CeO₂(111): A Combined Modulation Excitation DRIFTS and Density Functional Theory Study

Jakob Weyel¹ · Marc Ziemba¹ · Christian Hess¹

Accepted: 15 February 2022 / Published online: 1 March 2022
© The Author(s) 2022

Abstract

In this work we elucidate the main steps of the CO oxidation mechanism over Au/CeO₂(111), clarifying the course of CO adsorption at a broad variety of surface sites as well as of transmutations of one CO species into another. By combining transient spectroscopy with DFT calculations we provide new evidence that the active centers for CO conversion are single gold atoms. To gain insight into the reaction mechanism, we employ Modulation Excitation (ME) DRIFT spectroscopy in combination with the mathematical tool of Phase Sensitive Detection to identify the active species and perform DFT calculations to facilitate the assignments of the observed bands. The transient nature of the ME-DRIFTS method allows us to sort the observed species temporally, providing further mechanistic insight. Our study highlights the potential of combined transient spectroscopy and theoretical calculations (DFT) to clarify the role of adsorbates observed and to elucidate the reaction mechanism of CO oxidation over supported gold and other noble-metal catalysts.

Keywords Gold-ceria · In situ spectroscopy · Transient spectroscopy · CO oxidation · Modulation excitation spectroscopy (MES) · Phase sensitive detection (PSD) · DRIFTS · DFT

1 Introduction

Ceria, especially in combination with noble metal nanoparticles, is a widely used catalyst for oxidation reactions such as (preferential) CO oxidation or the (reverse) water–gas shift reaction [1–6]. Gold in particular has proven to be a valuable choice for stable and high performing catalyst systems [7–10]. Ceria, chosen as the supporting material in this study, is known to exhibit extensive dynamics in creating and annihilating (oxygen) defects that are of great importance for the proposed Mars-van-Krevelen mechanism of CO oxidation over Au/CeO₂ [5, 6, 11]. Its detailed mechanistic understanding is motivated by the CO oxidation as a prototypical reaction for heterogeneous catalysis [12] but also because of its technical relevance for the three-way catalytic converter [13] as well as its potential usage for CO₂

activation in the context of future carbon capture and usage (CCU) processes [14, 15]. Due to its importance for CO oxidation, this study focuses on the signals and the temporal behavior of CO adsorbates that are readily accessible via DRIFT spectroscopy. The CO spectral region exhibits valuable information concerning the state of adsorbed CO, including its bonding partner, its geometry as well as the surface termination and topology of the adsorption site. These parameters of CO adsorbates, that have also been a topic of one of our previous studies [6] are still under debate in literature [6, 16–23].

Although CO oxidation over supported noble metal catalysts has been investigated for a long time and in numerous studies, a profound understanding of the dynamics of the different CO adsorbate structures has not been achieved to date. To this end, new mechanistic insight may be expected from a combination of transient time-resolved DRIFT spectra with theoretical calculations of possible adsorbate structures such as vibrational frequencies and adsorption energies.

The special DRIFTS approach chosen in this study is depicted in Fig. 1. We use Modulation Excitation Spectroscopy (MES) in combination with data processing via Phase Sensitive Detection (PSD), a technique first introduced by Baurecht and Fringeli in 2001 [24]. Following their publication,

Jakob Weyel and Marc Ziemba have contributed equally.

✉ Christian Hess
christian.hess@tu-darmstadt.de

¹ Eduard-Zintl-Institute of Inorganic and Physical Chemistry, Technical University of Darmstadt, Alarich-Weiss-Str. 8, 64287 Darmstadt, Germany

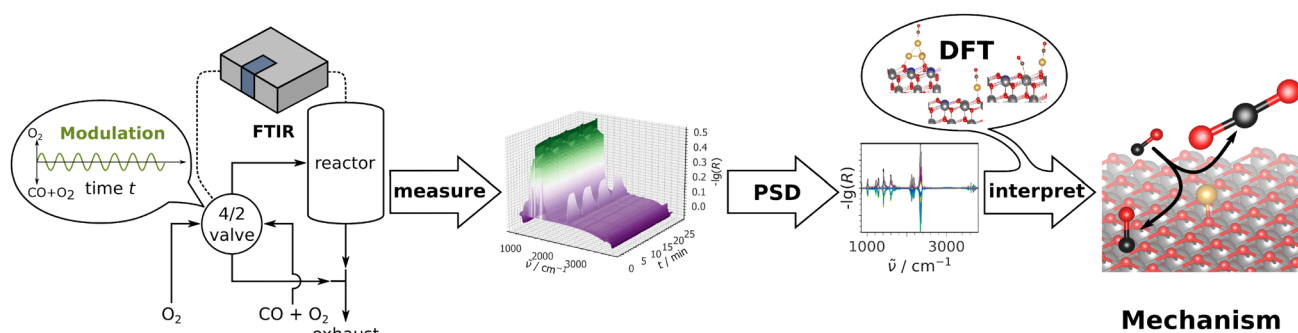


Fig. 1 Scheme of the experimental ME-DRIFTS setup, the data processing of the measured ME into PSD spectra, and the combination of these experimental spectra with DFT results allowing for new mechanistic insights. For details see text

interesting findings were made via the MES-PSD approach, especially in the field of heterogeneous catalysis, shining new light on the mechanistic course of reactions under consideration [25]. In previous studies, ME-DRIFTS was applied to (preferential) CO oxidation over supported catalysts including ceria as well [1, 16, 22, 26, 27].

MES and PSD are used to extract the dynamics from time-resolved spectra during periodic modulation of one process variable (in our case the concentration of one reactant) and to separate it from all time-constant signals (spectator species) as well as from the statistical background noise, thus providing valuable information on active species often hidden in conventional spectra. This is achieved via Fourier transformation of the time-resolved into phase-resolved spectra according to Eq. (1):

$$I(\tilde{\nu}, \varphi) = 2/T \int_{t_0}^{t_0+T} I(\tilde{\nu}, t) \cdot \sin(\omega t + \varphi) dt \quad (1)$$

with the signal intensity *I*, wavenumber $\tilde{\nu}$, duration of one period *T*, phase shift φ , time *t*, and the modulation frequency ω . After comparing different modulation functions and weighing the advantages and disadvantages, a sinusoidal modulation function was used in this work for reasons of simpler calculability. The DFT approach allows the calculation of IR active vibrational frequencies as well as their respective adsorption energies [6, 28]. As will be illustrated below for Au/CeO₂, the combination of transient ME-DRIFTS with theoretical DFT studies allows to obtain a more profound understanding of the first reaction steps of CO oxidation and especially the crucial CO adsorption processes.

2 Experimental Section

2.1 Catalyst Preparation and Characterization

Preparation and characterisation of the polycrystalline ceria catalyst used in this study was described in our previous work [5, 29, 30]. Summarizing, cerium nitrate hexahydrate (Alfa Aesar, 99.5%) is calcined for 12 h at 600 °C (ramp of 6 °C/min). After being cooled to room temperature, the powder is sieved (200 μm) and calcined a second time according to the protocol mentioned above. Ceria polyhedra were obtained commercially (Sigma Aldrich, <25 nm (BET)). In both cases, the gold loading was achieved by utilizing electrolyte deposition of a 10⁻³ M H₂AuCl₄ · 3 H₂O aqueous solution.

As reported previously, the commercial ceria sample exhibits polyhedral particles with a specific surface area of 36 m²g⁻¹, and the sample prepared by decomposition of cerium nitrate consists of ceria sheets with a specific surface area of 57 m²g⁻¹ [4, 31]. Both samples show a CeO₂(111) surface termination, but the sheets additionally possess stepped CeO₂(111) sites [4, 31]. The gold loading was confirmed by ICP-OES, revealing a gold content of 0.31 wt% for the sheets and 0.27 wt% for the polyhedra [31]. Furthermore, our previous study on Au/CeO₂(111) sheets has revealed a large dispersion of gold due to presence of single atoms and/or smaller clusters as probed by the CO-Au vibrations using DRIFTS [6].

2.2 Modulation Excitation (ME) DRIFTS

ME-DRIFTS was performed on a Vertex 70 spectrometer (Bruker) equipped with a liquid nitrogen cooled mercury cadmium telluride (MCT) detector and a commercial reaction cell (Praying Mantis™ High Temperature Reaction Chamber, Harrick Scientific Products) with infrared transparent KBr windows. Please note, that a more detailed description of our basic DRIFTS setup was already given in our previous studies [6, 32], while the additionally needed MES setup (gas pipelines, communication channels, data processing) is schematically depicted in Fig. 1.

For our measurements, 25–35 mg was placed in a stainless steel sample holder (\varnothing : 8 mm; depth: 0.5 mm). Due to the cell geometry and the overflow of the sample, the exact weight of the sample has hardly any influence on the catalytic activity. As background, the catalyst itself was used after 15 min pretreatment in O_2 atmosphere (100 mL min^{-1} of 10 mol% O_2 in Argon) at the reaction temperature of 37 °C and a subsequent gas phase modulation procedure (identical to the desired experiment), which ensures a reproducible state of the sample. The gas atmosphere during the background measurement consisted of 10 mol% O_2 in Ar (flow rate: 100 mL min^{-1}). For our measurements we used the rapid scan mode extension of the spectrometer software OPUS 7.2. Spectra were measured from 850 to 3800 cm^{-1} with a resolution of 0.5 cm^{-1} , an aperture of 8 mm and a mirror speed of 40 kHz. A Valco Instruments 4/2 valve (Model E2CA, version ED), communicating with the Vertex 70, is used to rapidly switch the gas flows, which are set via digital mass flow controllers (MFCs, Bronkhorst).

During ME-DRIFTS, the sample is exposed to a feed with constant O_2 content of 10 mol% of the total flow, while a CO flux is pulsed over the sample changing from 0 to 2 mol% (total flow rate: 100 mL/min; residual: Ar), resulting in a conversion of 3.4% for the sheets and of 1.2% for the polyhedra. Switching the valve position initially resulted in a square wave modulation behavior of the CO concentration but due to the residence time behavior of the setup it is better fitted by a sine wave as shown in Fig. 1. These diluted concentrations were chosen to keep the turnover low and to eliminate the influence of possible transport effects.

The following gases are used: CO (99.997%, Westfalen), O_2 (99.999%, Westfalen), and argon (99.996%, Westfalen). One measurement series consisted of 20 periods, with a duration of 374.2 s each. For each spectrum, five consecutive interferograms were averaged, so that one spectrum is acquired approximately every 1.5 s. To estimate potential uncertainties of the via PSD derived time values, the MES experiment on Au/CeO₂ sheets was exemplary executed three times. This resulted in a maximum deviation of time values of 3 s, as determined based on the signal at 2092 cm^{-1} . The other signals discussed show a maximum

deviation of 1 or 2 s (see Table S1). For some signals the determining factor is the time resolution between two successive measurements of 1.5 s, for some it is the maximum deviation (see Table S1).

Intensities and peak positions were checked multiple times and found to be constant for all of the measured datasets.

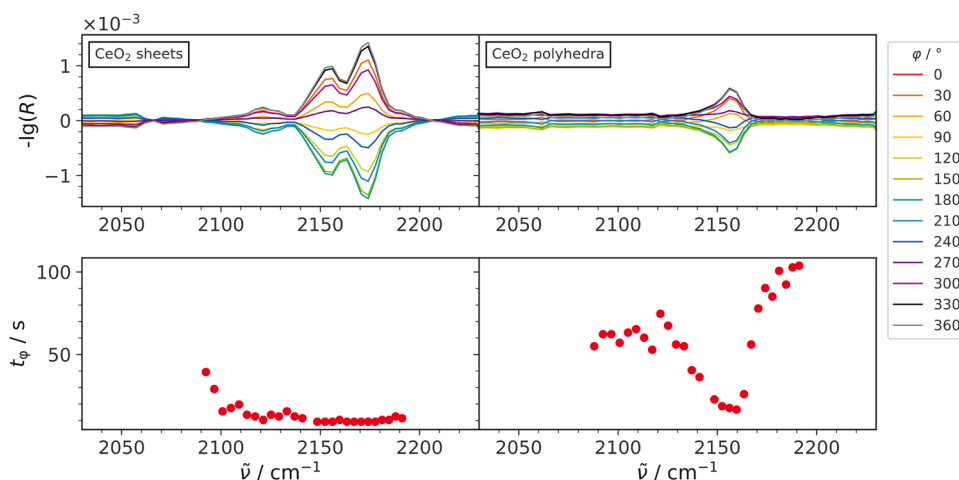
2.3 Density Functional Theory (DFT)

The approach and methods used in this study were described earlier [6, 30]. Briefly, calculations were performed using the spin-polarized DFT + U approach as implemented in the Vienna Ab initio Simulation Package (VASP, Version 5.3.5, <https://www.vasp.at/>), with the generalized gradient approximation of Perdew, Burke and Ernzerhof (PBE) [33] and an U_{eff} parameter of 4.5 eV for the Ce 4f states (PBE + U/4.5 eV). The Ce (4f, 5 s, 5p, 5d, 6 s), O (2 s, 2p), Au (5d, 6 s) and C (2 s, 2p) electrons were explicitly treated as valence states within the projector augmented wave (PAW) method [34] with a plane-wave cutoff of 400 eV, whereas the remaining electrons were treated as part of the atomic cores. The CeO₂(111) surface was modelled by supercells with (3 × 3) periodicities with the calculated ceria bulk equilibrium lattice constant (5.484 Å) [30]. A slab of three trilayers, separated by at least a 10 Å-thick vacuum layer, was used. The slab thickness has been chosen based on the convergence of the calculated surface energy. The sampling of the Brillouin zone is realized by a (2 × 2 × 1) Monkhorst–Pack grid [35]. All atoms in the bottom trilayer were fixed at their optimized bulk-truncated positions during geometry optimization, whereas the rest of the atoms were allowed to fully relax. Total energies and forces were calculated with a precision of 10⁻⁶ eV and 10⁻² eVÅ⁻¹ for electronic and force convergence, respectively. After relaxation a vibrational analysis was performed by calculating the mass-weighted Hessian matrix using density functional perturbation theory (DFPT).

3 Results and Discussion

Although many features of the CO oxidation mechanism over Au catalysts were clarified previously, some important details are still missing, such as processes related to the initial CO adsorption and the subsequent adsorbate rearrangement. To address these processes in detail, we will focus on the CO adsorbate region ranging from 2000 to 2250 cm^{-1} , while other spectral regions (carbonates, hydroxyl groups) will not be considered in this work. For completeness, full PSD spectra as well as time-resolved spectra of the CO region of all samples studied are shown in the Supporting Information (see Figures S1–S4, S6–S9).

Fig. 2 Top: PSD spectra of the CO region of CeO₂ sheets (left) and polyhedra (right) after removal of gas-phase contributions. Bottom: Corresponding time shifts of individual spectral positions



Comparing the spectra of the two bare ceria samples (see top of Fig. 2), it is apparent that the sheets exhibit three signals (2122 cm⁻¹, 2156 cm⁻¹ and 2171 cm⁻¹), but the polyhedra only one signal at 2156 cm⁻¹. The latter is assigned to CO adsorbed onto the ideal CeO₂(111) surface [19, 20, 36]. The band located at higher wavenumbers, i.e. at 2171 cm⁻¹, indicates a stronger interaction of CO with the surface, and can therefore be attributed to CO adsorbed on reduced CeO₂(111), in agreement with the literature [18, 36]. The location of the band at 2122 cm⁻¹ is fully consistent with Ce³⁺ related electronic transitions [17, 37].

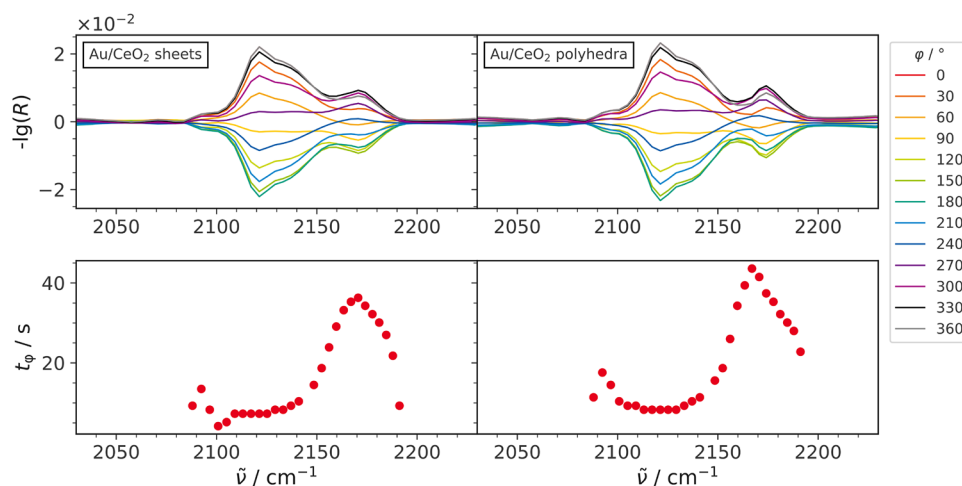
Although both ceria samples show a (111) termination, the sheets exhibit additional steps (see above), which have been shown to have a positive influence on the reduction behavior [31]. Thus the sheets possess more oxygen defects than the polyhedra, which is clearly reflected in the vibrational signature of the CO region.

In addition to the spectral position of each signal, MES-PSD is furthermore able to provide information on each signal's transient behavior via time values, which indicate the appearance of each signal relative to the others within the external modulation period. The time values shown at the bottom of Fig. 2 indicate differences between the bare ceria samples. In fact, in case of the sheets, signals appear within 11–15 s after turning on the reaction gas atmosphere, whereas for lower wavenumbers on the border of the sampled region, where no bands can be seen, a steep increase of the time values is visible. For the polyhedral-related band a time shift of about 13–20 s is detected. Again, outside the region of this feature, time values steeply increase up to roughly 70 s for wavenumbers lower than 2156 cm⁻¹ and 100 s for wavenumbers higher than that. This increase can be related to a transition from the CO adsorbate signal to the background surrounding it, as can be seen in Figure S5 but will not be further addressed here as the background holds no useful information. The time values of the signal at 2156 cm⁻¹ appear at 11 s for the sheets and at 15 s for the

polyhedra, respectively. Please note that these values contain an experimental uncertainty of 1.5 s due to the rate of spectra measurement (for details see Experimental) as well as a maximum deviation between different measurements of 1 s (see Table S1). Thus the observed difference of the time values of the 2156 cm⁻¹ signal for ceria sheets and polyhedra appears significant; it may originate from the fact that the surrounding of a signal has an influence on these time values. The observed deviation for the same species on sheets and polyhedra might also be due to the fact that the surrounding of a signal has an influence on these time values. In case of ceria sheets, the signal is surrounded by other peaks exhibiting about the same time shift. In case of polyhedra, the signal stands alone and is weaker compared to the sheets. This weakness is expected to be partly due to the lower surface area and thus a lower number of possible adsorption sites. However, since the gold-loaded samples (see Fig. 3) show almost the same intensity at the same surface areas as the bare ceria samples, it becomes apparent that there is also a contribution from other effects, e.g. particle shape and degree of reduction. Via an overlap, the neighboring signals or even the background might influence the regarded signal according to the relative intensity of it and the overlapping contribution, thus a mixing of time values occurs, as has been already described elsewhere [38]. Therefore it might as well be the case that these overlap effects lead to different time values of the same species on ceria sheets and polyhedra. Nevertheless, these discrepancies neither affect the interpretations made here nor the mechanistic discussion of the results at the end.

The top of Fig. 3 depicts the PSD spectra of gold-loaded ceria sheets (left) and polyhedra (right). For both samples, the spectra show a similar vibrational profile and are dominated by signals at about 2122 cm⁻¹ and 2171 cm⁻¹. The first signal corresponds to CO adsorbed onto a gold cluster, the second to CO adsorbed onto bare ceria, as discussed previously [6]. The signal at around 2171 cm⁻¹

Fig. 3 Top PSD spectra of the CO region of Au/CeO₂ sheets (left) and Au/CeO₂ polyhedra (right) after removal of gas-phase contributions. Bottom Corresponding time shifts of individual spectral positions



shows a slight asymmetry towards lower wavenumbers, which is less pronounced for the polyhedra than for the sheets. Vice versa the polyhedra samples exhibit a small asymmetry towards higher wavenumbers leading to a shift of the signal's maximum to 2174 cm⁻¹. A comparison to the spectra of the bare ceria samples in Fig. 2 shows, that the dominant CO-related band at about 2156 cm⁻¹ appears to be blueshifted to 2171 cm⁻¹ for the gold-loaded samples. In agreement with previous studies, this behavior is attributed to the increased number of defects formed in the presence of gold, and consistent with the observation of the 2171 cm⁻¹ band on the bare ceria sheets (see above) [39]. In this context, our previous studies at the same gas concentrations also revealed the presence of defects on the Au/sheets by means of *operando* Raman and UV–Vis spectroscopy [5]. Furthermore, both spectra show a broad contribution at about 2133 cm⁻¹ and a small foothill at about 2092 cm⁻¹. Please note that a significant contribution of electronic transitions of reduced ceria, which may be expected in the region at around 2125 cm⁻¹ [17], can be excluded for the gold-loaded samples based on previous isotope experiments [6].

Interestingly, the time values of the gold-loaded catalysts, exhibit significant differences to the bare ceria samples. In fact, as can be seen at the bottom of Fig. 3 the CO@CeO₂ signals at around 2171 cm⁻¹ exhibit a time shift of 30–40 s, compared to 10–20 s for bare ceria. The CO-Au@CeO₂ signals on the other hand show time shifts of about 5–10 s that are nearly the same for both gold-loaded sheets and polyhedra. The increased time value of the CO@CeO₂ signals in the presence of gold may be rationalized by a different type of adsorption (see below). This is supported by the observed increase in intensity by a factor of about 10 when gold is added, suggesting that there is another mechanism at work that overshadows simple adsorption from the gas phase. A possible scenario may be based on a spillover of unreacted CO from gold particles to the ceria surface, comparable to

the CO₂ formation mechanism proposed in the literature [2, 40].

According to previous studies, charge and coordination of gold have a major influence on the CO adsorption energy on Au/CeO₂ systems [41–43]. It is therefore conceivable that larger gold clusters lead to a spillover of CO to the surface, because in this case adsorption on the support may be preferred [36, 43]. On the other hand, studies show that Au single sites are also formed dynamically from larger gold clusters under reaction conditions, therefore being referred to as pseudo-single sites [11, 41]. To this end, based on DFT calculations the adsorption of CO onto such a gold single or pseudo-single site ($E_{\text{ads,CO}}(\text{Au}_1) = -2.58$ eV) instead of ceria ($E_{\text{ads,CO}}(\text{CeO}_2) = -0.19$ eV) [6] is energetically much more attractive [6, 40], thus a spillover seems energetically unfavorable at first, where the adsorption energies are consistent with previous studies [20, 44]. However, it is conceivable that CO adsorbed on gold may orient itself towards the ceria surface and be displaced by a second CO from the gas phase. This assumption is supported by our DFT calculations shown in the second structure in Fig. 4 (replaced single site) confirming (i) the displacement of CO previously adsorbed at a gold single site by another CO molecule from the gas phase and (ii) its relocation and migration onto the ceria surface ($E_{\text{ads, repl. CO}}(\text{CeO}_2) = -0.106$ eV).

This ensemble of two CO adsorbates, one adsorbed onto a single gold atom, the other to the adjacent ceria surface, is characterized by two vibrational frequencies at 2083 and 2096 cm⁻¹ (see Fig. 4). These two frequencies cannot be easily separated because vibrational analysis yields primarily two stretching modes involving both CO molecules. One where both CO bonds oscillate in phase and one where they oscillate in opposing phases. This is indicative for dipolar interactions, as described in the literature [45–49].

A further distribution of CO molecules located at the gold-ceria interface is expected, since CO has a more favorable binding energy of -0.19 eV on the bare ceria support.

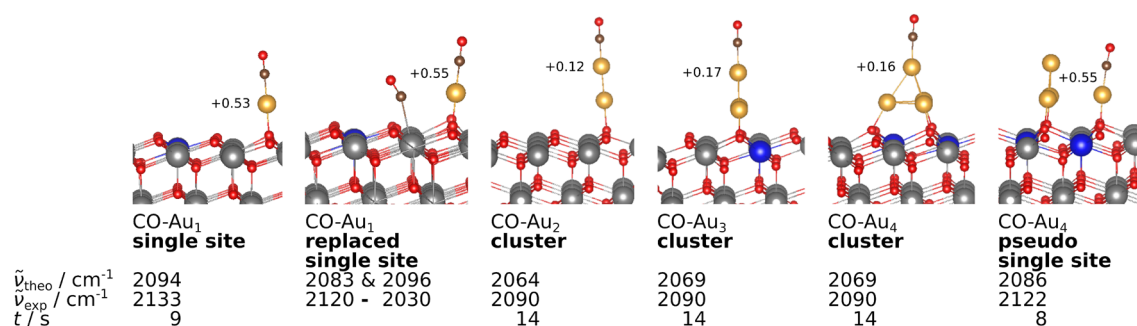


Fig. 4 Top: Most stable structures for CO adsorbed on Au₁₋₄/CeO₂(111) structures from DFT together with the Bader charges (ΔQ , in $|e|$) of the gold atom in direct contact with CO. Bottom: Cal-

culated and experimental vibrational frequencies of adsorbed CO, as well as the corresponding time values for ceria sheets derived from PSD calculations

This additional step offers an explanation for the considerably later appearance of the CO@CeO₂ signals when gold is involved. Hence, based on the observed time-shifts of the CO@CeO₂ signals, the following mechanism for CO adsorption on Au/CeO₂ may be proposed: (i) CO adsorption onto gold, (ii) subsequent spillover and/or displacement by gaseous CO, and (iii) CO movement away from the gold-ceria interface, leading to its dispersion on the carrier. Because of the easier adsorption of CO to gold than to CeO₂, such a spillover/displacement mechanism may largely facilitate the surface loading with CO molecules, thus accelerating the CO adsorption process. Such a scenario is supported by the signal intensity for the bands at 2156 and 2171 cm⁻¹, which is roughly ten times higher for the gold loaded than for the bare ceria samples (see Figs. 2 and 3).

The signal of gaseous CO₂ (not shown here) appears after ~20 s (maximum intensity) for the sheets and ~21 s for the polyhedra. As CO₂ formation occurs significantly before the appearance of the intense CO@CeO₂ signals, it stands to reason that product formation is independent of the postulated spillover/displacement processes. Nonetheless, a simultaneous accumulation of CO on ceria sites might still be possible, but due to the expected low intensities for such a species (compare the intensities in Figs. 2 and 3) their signals might either be very weak or completely absent. Based on this fact and the spillover/displacement processes, we may now exclude CO adsorbed on ceria to be active even if it shows an increased intensity in the PSD spectra when gold is present (see Fig. 3). This is in accordance with the literature, where the inactivity of bare ceria at the chosen reaction temperature has been clearly evidenced [5]. Thus CO adsorption on gold appears to be strictly necessary for catalytic activity.

Looking more closely at the spectral region attributed to CO adsorbed on gold, the vibrational profile surrounding the signal at around 2122 cm⁻¹ in Fig. 3 clearly indicates several contributions. These may be rationalized by different CO-Au species existing on the surface, ranging from

CO adsorbed on a single gold atom (single site), which is considered to be the most active species [6], up to larger gold clusters consisting of multiple atoms. To illustrate the effect of cluster size, the vibrational frequencies and the respective adsorption energies of several model structures of CO on gold (Au₁ to Au₄) were calculated using DFT (see Fig. 4). The structures for Au₂ and Au₃ were taken from Ghosh et al. [40], whereas Au₁ and Au₄ were part of our previous studies [6].

According to literature, the signals at 2122 cm⁻¹ and 2133 cm⁻¹ can be assigned to CO adsorbed to gold single sites: the signal at 2133 cm⁻¹ was often associated to CO on a single gold atom on the surface [6], while the one at 2122 cm⁻¹ is assigned to CO on a so called pseudo-single site, where one gold atom is slightly removed from a larger cluster, thus forming the CO adsorption site [6]. The single sites might as well be formed by such a dynamic process as there has been evidence, that completely isolated gold atoms tend to block the adsorption of CO, due to a negatively charged Au atom [11, 40]. Thus in the following we will refer to these sites as pseudo-single sites. The dynamic formation of pseudo-single sites has been demonstrated by earlier theoretical studies [6, 11]. CO on larger gold particles gives rise to a small shoulder at 2092 cm⁻¹ (see Fig. 3). According to our DFT calculations, it seems to be irrelevant whether the cluster comprises two, three or four atoms. This is illustrated in Fig. 4, showing quite similar vibrational frequencies of 2064 and 2069 cm⁻¹ for different cluster sizes. This underlines the impact of the charge of the gold atom on which the CO is located on the vibrational frequency, since this is lower for the latter structures. Continuing this thought, further contributions to this signal cannot be ruled out completely, as there may be contributions due to charge transfer from vacancies (formed during reaction) to gold clusters, changing the bond strength of adsorbed CO there. Computational evidence for such a bond weakening has been given by Ghosh et al. [40]. Experiments by Manzoli et al. provide

Fig. 5 Proposed mechanisms for **a** CO₂ formation on an exemplary gold (pseudo-) single site not showing the rest of the larger gold cluster and **b** CO spillover, leading to the formation of CO@CeO₂ species. For details see text

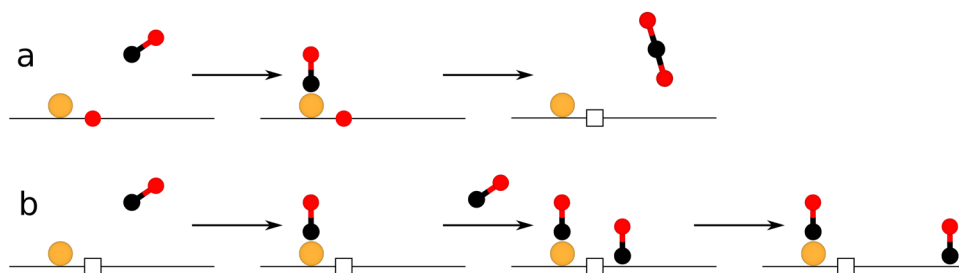


Table 1 Observed signals and their time values for gold-loaded and bare ceria sheets and polyhedra (in brackets)

$\tilde{\nu}/\text{cm}^{-1}$	$t(\text{Au/CeO}_2)/\text{s}$	$t(\text{CeO}_2)/\text{s}$	Assignment
2092	14 (18)	– (–)	CO-Au _n cluster
2122	8 (9)	– (–)	CO-Au pseudo-single site
2122	– (–)	12 (–)	Ce ³⁺ electr. transition
2133	9 (10)	– (–)	CO-Au pseudo-single site
2156	24 (26)	11 (15)	CO@CeO ₂ , ideal
2171	34 (39)	10 (–)	CO@CeO ₂ , reduced
2359	20 (21)	– (–)	CO ₂

experimental indications of red-shifted CO adsorbate signals on reduced gold-ceria catalysts during CO oxidation in the regarded spectral region [21].

Combining the above results on peak positions and signal intensities as well as the respective times extracted via PSD, a mechanistic picture of the first steps of CO oxidation on Au/CeO₂ can be drawn (see Fig. 5). Table 1 summarizes the relevant species and their assignment for sheets and polyhedra samples.

From Table 1 it is apparent, that the adsorption mechanism follows the same path for sheets and polyhedra. Thus, both samples will be discussed together in the following. A visual representation of our findings is shown in Fig. 5. First the adsorption of CO on pseudo-single gold sites occurs (7–10 s), giving rise to signals at 2133 and 2122 cm⁻¹, respectively. Conversion of these CO molecules seems to be the main reaction route towards CO₂. Next, the signal at 2092 cm⁻¹ is detected, which is associated with CO on larger gold clusters and/or their CO adsorption dynamics due to the reduction state of the surface (~ 14 s for sheets, ~ 15 s for polyhedra). Due to its low intensity in PSD spectra it is unlikely that these CO molecules play a major role in the reaction. The fact that this feature shows at least some intensity may be attributed to (limited) dynamics of adsorption and desorption when changing the gas atmosphere.

The next signal observed corresponds to gas phase CO₂, the product of the reaction, which is formed at 20 s for sheets and 21 s for polyhedra. The proposed mechanism for CO₂ formation is shown in Fig. 5a. Briefly summarized, it consists of (i) CO adsorption onto an active gold site,

and (ii) formation and dissociation of CO₂ via a proposed O_{lattice}-Au⁺-CO species [6, 11, 40, 50].

After this, the signals of CO on bare ceria are detected. Among these, first the signal of CO on the ideal surface appears at 24 (sheets) or 26 s (polyhedra), and then the signal of CO on the reduced surface at 34 (sheets) or 39 s (polyhedra). As discussed above, the late appearance of these signals indicates that they are not involved in the reaction mechanism but emerge due to a spillover/displacement mechanism, distributing unreacted CO adsorbed on gold particles to the surrounding ceria, as depicted in Fig. 5b. This spillover/displacement process may occur instead of a reaction because of a possible depletion of the CeO₂ surface of oxygen needed for CO oxidation. This depletion is indicated by the dominant CO@CeO₂ signal at 2171 cm⁻¹ which is assigned to a reduced surface. While being unreactive on the ceria surface, after spillover/displacement, the CO molecules may resemble those on bare ceria sheets (see Fig. 2) and exhibit adsorption–desorption dynamics upon exposure to changing gas atmospheres, thus explaining their intensity in PSD spectra.

4 Conclusion

Summarizing this work, we were able to further elucidate the reaction pathway of the CO oxidation, a prototype reaction in heterogeneous catalysis, using gold-loaded ceria catalysts as a showcase. We chose Modulation Excitation (ME) DRIFT Spectroscopy, which enables detailed analysis of the adsorbates as well as the adsorption and reaction process, focusing on CO and CO₂ signals. In combination with Phase Sensitive Detection (PSD), our transient experiments provide new information on the active species and their temporal order. Combining this experimental data with findings from DFT (structures, vibrational frequencies), allowed us to clarify the reaction sequence of CO adsorption and reaction on Au/CeO₂ catalysts.

Our results confirm the activity of dynamically formed pseudo-single sites. Furthermore, we show that CO adsorbed onto larger clusters of more than two gold atoms as well as CO adsorbed onto ceria is not involved in the reaction mechanism. CO on larger clusters is excluded as active species

due to its low intensity in PSD spectra. CO adsorbed to the ceria support, showed high intensity signals in PSD spectra. However, its participation in the reaction was excluded due to its late appearance in the mechanism, i.e., after that of the product CO₂. Based on a comparison with bare ceria, its signal intensity is rationalized by a spillover/displacement mechanism of unreacted CO from gold to the reduced and oxygen-depleted ceria surface.

Finally, our approach clearly demonstrates that the combination of transient spectroscopic techniques, such as ME-DRIFTS, with DFT calculations can greatly enhance our understanding of reaction mechanisms in heterogeneous catalysis.

Supplementary Information The online version contains supplementary material available at <https://doi.org/10.1007/s11244-022-01599-1>.

Acknowledgements We thank M. Verónica Ganduglia-Pirovano for fruitful discussions, and Karl Kopp for technical support. Calculations for this research were conducted on the Lichtenberg high performance computer of the TU Darmstadt. Jakob Weyel gratefully acknowledges a scholarship from the Fonds der Chemischen Industrie im Verband der Chemischen Industrie e.V.

Authors contributions All authors contributed to the conception and design of the study. Experiments were performed by Jakob Weyel, DFT calculations by Marc Ziemba. The first draft of the manuscript was written by Jakob Weyel. All authors commented and edited the first and following versions of the manuscript. All authors read and approved the final manuscript. Christian Hess was responsible for supervision and funding acquisition.

Funding Open Access funding enabled and organized by Projekt DEAL. Jakob Weyel gratefully acknowledges a scholarship from the Fonds der Chemischen Industrie im Verband der Chemischen Industrie e.V.

Code availability The software used for calculation of PSD spectra is available at https://github.com/Ja-We/Phase_Sensitive_Detection_for_Spectroscopy.

Declarations

Conflict of interest The authors do not have conflict of interest to declare.

Open Access This article is licensed under a Creative Commons Attribution 4.0 International License, which permits use, sharing, adaptation, distribution and reproduction in any medium or format, as long as you give appropriate credit to the original author(s) and the source, provide a link to the Creative Commons licence, and indicate if changes were made. The images or other third party material in this article are included in the article's Creative Commons licence, unless indicated otherwise in a credit line to the material. If material is not included in the article's Creative Commons licence and your intended use is not permitted by statutory regulation or exceeds the permitted use, you will need to obtain permission directly from the copyright holder. To view a copy of this licence, visit <http://creativecommons.org/licenses/by/4.0/>.

References

- Kydd R, Ferri D, Hug P et al (2011) Temperature-induced evolution of reaction sites and mechanisms during preferential oxidation of CO. *J Catal* 277:64–71. <https://doi.org/10.1016/j.jcat.2010.10.009>
- Wang LC, Widmann D, Behm RJ (2015) Reactive removal of surface oxygen by H₂, CO and CO/H₂ on a Au/CeO₂ catalyst and its relevance to the preferential CO oxidation (PROX) and reverse water gas shift (RWGS) reaction. *Catal Sci Technol* 5:925–941. <https://doi.org/10.1039/C4CY01030B>
- Meunier FC, Tibiletti D, Goguet A et al (2005) On the reactivity of carbonate species on a Pt/CeO₂ catalyst under various reaction atmospheres: application of the isotopic exchange technique. *Appl Catal A Gen* 289:104–112
- Schilling C, Hess C (2019) Elucidating the role of support oxygen in the water-gas shift reaction over ceria-supported gold catalysts using operando spectroscopy. *ACS Catal* 9:1159–1171. <https://doi.org/10.1021/acscatal.8b04536>
- Schilling C, Hess C (2018) Real-time observation of the defect dynamics in working Au/CeO₂ catalysts by combined operando Raman/UV–vis spectroscopy. *J Phys Chem C* 122:2909–2917. <https://doi.org/10.1021/acs.jpcc.8b00027>
- Schilling C, Ziemba M, Hess C, Ganduglia-Pirovano MV (2020) Identification of single-atom active sites in CO oxidation over oxide-supported Au catalysts. *J Catal* 383:264–272. <https://doi.org/10.1016/j.jcat.2020.01.022>
- Haruta M (2003) When gold is not noble: catalysis by nanoparticles. *Chem Rec* 3:75–87. <https://doi.org/10.1002/tcr.10053>
- Haruta M (2002) Catalysis of gold nanoparticles deposited on metal oxides. *CATTECH* 6:102–115. <https://doi.org/10.1023/A:1020181423055>
- Bond GC (2002) Gold: a relatively new catalyst. *Catal Today* 72:5–9. [https://doi.org/10.1016/S0920-5861\(01\)00522-3](https://doi.org/10.1016/S0920-5861(01)00522-3)
- Hutchings GJ (2018) Heterogeneous gold catalysis. *ACS Cent Sci* 4:1095–1101. <https://doi.org/10.1021/acscentsci.8b00306>
- Wang Y-G, Mei D, Glezakou V-A et al (2015) Dynamic formation of single-atom catalytic active sites on ceria-supported gold nanoparticles. *Nat Commun* 6:6511. <https://doi.org/10.1038/ncomms7511>
- Freund H-J, Meijer G, Scheffler M et al (2011) CO oxidation as a prototypical reaction for heterogeneous processes. *Angew Chemie Int Ed* 50:10064–10094. <https://doi.org/10.1002/anie.201101378>
- Diwell AF, Rajaram RR, Shaw HA, Truex TJ (1991) The role of ceria in three-way catalysts. *Stud Surf Sci Catal* 71:139–152. [https://doi.org/10.1016/S0167-2991\(08\)62975-4](https://doi.org/10.1016/S0167-2991(08)62975-4)
- Rezvani A, Abdel-Mageed AM, Ishida T et al (2020) CO₂ Reduction to methanol on Au/CeO₂ catalysts: mechanistic insights from activation/deactivation and SSITKA measurements. *ACS Catal* 10:3580–3594. <https://doi.org/10.1021/acscatal.9b04655>
- Vovchok D, Zhang C, Hwang S et al (2020) Deciphering dynamic structural and mechanistic complexity in Cu/CeO₂/ZSM-5 catalysts for the reverse water-gas shift reaction. *ACS Catal* 10:10216–10228. <https://doi.org/10.1021/acscatal.0c01584>
- Fernández-García S, Collins SE, Tinoco M et al (2019) Influence of 111 nanofaceting on the dynamics of CO adsorption and oxidation over Au supported on CeO₂ nanocubes: an operando DRIFT insight. *Catal Today* 336:90–98. <https://doi.org/10.1016/j.cattod.2019.01.078>
- Daly H, Ni J, Thompsett D, Meunier F (2008) On the usefulness of carbon isotopic exchange for the operando analysis of metal–carbonyl bands by IR over ceria-containing catalysts. *J Catal* 254:238–243. <https://doi.org/10.1016/j.jcat.2007.12.013>

18. Yang C, Yu X, Heißler S et al (2017) Surface faceting and reconstruction of ceria nanoparticles. *Angew Chemie Int Ed* 56:375–379. <https://doi.org/10.1002/anie.201609179>
19. Wöll C (2020) Structure and chemical properties of oxide nanoparticles determined by surface-ligand IR spectroscopy. *ACS Catal* 10:168–176. <https://doi.org/10.1021/acscatal.9b04016>
20. Lustemberg PG, Plessow PN, Wang Y et al (2020) Vibrational frequencies of cerium-oxide-bound CO: a challenge for conventional DFT methods. *Phys Rev Lett* 125:256101. <https://doi.org/10.1103/PhysRevLett.125.256101>
21. Manzoli M, Boccuzzi F, Chiorino A et al (2007) Spectroscopic features and reactivity of CO adsorbed on different Au/CeO₂ catalysts. *J Catal* 245:308–315. <https://doi.org/10.1016/j.jcat.2006.10.021>
22. del Río E, Collins SE, Aguirre A et al (2014) Reversible deactivation of a Au/Ce_{0.62}Zr_{0.38}O₂ catalyst in CO oxidation: a systematic study of CO₂-triggered carbonate inhibition. *J Catal* 316:210–218. <https://doi.org/10.1016/j.jcat.2014.05.016>
23. Song W, Hensen EJM (2013) A computational DFT study of CO oxidation on a Au nanorod supported on CeO₂(110): on the role of the support termination. *Catal Sci Technol* 3:3020. <https://doi.org/10.1039/c3cy00319a>
24. Baurecht D, Fringeli UP (2001) Quantitative modulated excitation Fourier transform infrared spectroscopy. *Rev Sci Instrum* 72:3782–3792. <https://doi.org/10.1063/1.1400152>
25. Müller P, Hermans I (2017) Applications of modulation excitation spectroscopy in heterogeneous catalysis. *Ind Eng Chem Res* 56:1123–1136. <https://doi.org/10.1021/acs.iecr.6b04855>
26. Aguirre A, Barrios CE, Aguilar-Tapia A et al (2016) In-Situ DRIFT study of Au–Ir/ceria catalysts: activity and stability for CO oxidation. *Top Catal* 59:347–356. <https://doi.org/10.1007/s11244-015-0425-6>
27. Aguirre A, Zanella R, Barrios C et al (2019) Gold stabilized with iridium on ceria-niobia catalyst: activity and stability for CO oxidation. *Top Catal* 62:977–988. <https://doi.org/10.1007/s11244-019-01185-y>
28. Ziemba M, Hess C (2020) Influence of gold on the reactivity behaviour of ceria nanorods in CO oxidation: combining operando spectroscopies and DFT calculations. *Catal Sci Technol* 10:3720–3730. <https://doi.org/10.1039/D0CY00392A>
29. Schilling C, Ganduglia-Pirovano MV, Hess C (2018) Experimental and theoretical study on the nature of adsorbed oxygen species on shaped ceria nanoparticles. *J Phys Chem Lett* 9:6593–6598. <https://doi.org/10.1021/acs.jpcclett.8b02728>
30. Schilling C, Hofmann A, Hess C, Ganduglia-Pirovano MV (2017) Raman spectra of polycrystalline CeO₂: a density functional theory study. *J Phys Chem C* 121:20834–20849. <https://doi.org/10.1021/acs.jpcc.7b06643>
31. Ziemba M, Weyel J, Hess C (2022) Elucidating the mechanism of the reverse water–gas shift reaction over Au/CeO₂ catalysts using operando and transient spectroscopies. *Appl Catal B Environ* 301:120825. <https://doi.org/10.1016/j.apcatb.2021.120825>
32. Schilling C, Hess C (2017) CO oxidation on ceria supported gold catalysts studied by combined operando raman/UV–Vis and IR spectroscopy. *Top Catal* 60:131–140. <https://doi.org/10.1007/s11244-016-0732-6>
33. Perdew JP, Burke K, Ernzerhof M (1996) Generalized gradient approximation made simple. *Phys Rev Lett* 77:3865–3868. <https://doi.org/10.1103/PhysRevLett.77.3865>
34. Blöchl PE (1994) Projector augmented-wave method. *Phys Rev B* 50:17953–17979. <https://doi.org/10.1103/PhysRevB.50.17953>
35. Monkhorst HJ, Pack JD (1976) Special points for Brillouin-zone integrations. *Phys Rev B* 13:5188–5192. <https://doi.org/10.1103/PhysRevB.13.5188>
36. Yang C, Yin LL, Bebensee F et al (2014) Chemical activity of oxygen vacancies on ceria: a combined experimental and theoretical study on CeO₂(111). *Phys Chem Chem Phys* 16:24165–24168. <https://doi.org/10.1039/c4cp02372b>
37. Bozon-Verduraz F, Bensalem A (1994) IR studies of cerium dioxide: influence of impurities and defects. *J Chem Soc Faraday Trans* 90:653. <https://doi.org/10.1039/ft9949000653>
38. Hemmingsson F, Schaefer A, Skoglundh M, Carlsson P-A (2020) CO₂ methanation over Rh/CeO₂ studied with infrared modulation excitation spectroscopy and phase sensitive detection. *Catalysts* 10:601. <https://doi.org/10.3390/catal10060601>
39. Ziemba M, Ganduglia-Pirovano MV, Hess C (2021) Insight into the mechanism of the water–gas shift reaction over Au/CeO₂ catalysts using combined operando spectroscopies. *Faraday Discuss* 229:232–250. <https://doi.org/10.1039/C9FD00133F>
40. Ghosh P, Farnesi Camellone M, Fabris S (2013) Fluxionality of Au clusters at ceria surfaces during CO oxidation: relationships among reactivity, size, cohesion, and surface defects from DFT simulations. *J Phys Chem Lett* 4:2256–2263. <https://doi.org/10.1021/jz4009079>
41. Liu J-C, Wang Y-G, Li J (2017) Toward rational design of oxide-supported single-atom catalysts: atomic dispersion of gold on ceria. *J Am Chem Soc* 139:6190–6199. <https://doi.org/10.1021/jacs.7b01602>
42. Liu Y, Li H, Yu J et al (2015) Electronic storage capacity of ceria: role of peroxide in Aux supported on CeO₂(111) facet and CO adsorption. *Phys Chem Chem Phys* 17:27758–27768. <https://doi.org/10.1039/c5cp03394b>
43. Han Z-K, Gao Y (2015) A 2D–3D structure transition of gold clusters on CeO_{2-x} (111) surfaces and its influence on CO and O₂ adsorption: a comprehensive DFT + U investigation. *Nanoscale* 7:308–316. <https://doi.org/10.1039/C4NR03346A>
44. Thang HV, Maleki F, Tosoni S, Pacchioni G (2021) Vibrational properties of CO adsorbed on au single atom catalysts on TiO₂(101), ZrO₂(101), CeO₂(111), and LaFeO₃(001) surfaces: a DFT study. *Top Catal* 1:3. <https://doi.org/10.1007/s11244-021-01514-0>
45. Penschke C, Paier J, Sauer J (2013) Oligomeric vanadium oxide species supported on the CeO₂(111) surface: structure and reactivity studied by density functional theory. *J Phys Chem C* 117:5274–5285. <https://doi.org/10.1021/jp400520j>
46. Penschke C, Paier J, Sauer J (2018) Vanadium oxide oligomers and ordered monolayers supported on CeO₂ (111): structure and stability studied by density functional theory. *J Phys Chem C* 122:9101–9110. <https://doi.org/10.1021/acs.jpcc.8b01998>
47. Crossley King AD (1980) Adsorbate island dimensions and interaction energies from vibrational spectra: CO on Pt{001} and Pt{111}. *Surf Sci* 95:131–155. [https://doi.org/10.1016/0039-6028\(80\)90132-6](https://doi.org/10.1016/0039-6028(80)90132-6)
48. González SR, Aymonino PJ, Piro OE (1984) Spectroscopic evidence of vibrational dipole–dipole coupling between nitrosyl groups in some nitroprussides. *J Chem Phys* 81:625–628. <https://doi.org/10.1063/1.447735>
49. Hollins P (1985) Influence of dipole coupling on the infrared spectra of adsorbed species and its significance for the interpretation of transmission spectra from supported metal catalysts. *Adsorpt Sci Technol* 2:177–193. <https://doi.org/10.1177/026361748500200304>
50. Camellone MF, Fabris S (2009) Reaction mechanisms for the CO oxidation on Au/CeO₂ catalysts: activity of substitutional Au³⁺/Au⁺ cations and deactivation of supported Au⁺ adatoms. *J Am Chem Soc* 131:10473–10483. <https://doi.org/10.1021/ja902109k>